International Journal of Pharmaceutics 413 (2011) 184–193

Contents lists available at ScienceDirect

International Journal of Pharmaceutics

journal homepage: www.elsevier.com/locate/ijpharm

Pharmaceutical Nanotechnology

Effect of wheat germ agglutinin density on cellular uptake and toxicity of wheat germ agglutinin conjugated PEG–PLA nanoparticles in Calu-3 cells

Yehong Shen[a,b], Jie Chen[a,b], Qingfeng Liu[a,b], Chengcheng Feng[a,b], Xiaoling Gao[c], Lu Wang[a,b], Qizhi Zhang[a,b,*], Xinguo Jiang[a,b]

[a] Department of Pharmaceutics, School of Pharmacy, Fudan University, Shanghai 201203, PR China
[b] Key Laboratory of Smart Drug Delivery, Ministry of Education & PLA, PR China, 201203
[c] Department of Pharmacology, College of Basic Medical Sciences, Shanghai Jiao Tong University, Shanghai 200025, PR China

ARTICLE INFO

Article history:
Received 2 January 2011
Received in revised form 11 April 2011
Accepted 13 April 2011
Available online 28 April 2011

Keywords:
WGA density
PEG–PLA nanoparticles
Calu-3 cells
Uptake efficiency
Cytotoxicity

ABSTRACT

Wheat germ agglutinin (WGA) modified PEG–PLA nanoparticles (WGA–NP) have demonstrated its potential for enhancing delivery of peptides into brain following intranasal administration. However, the effect of ligand density is less well known. WGA density may affect nanoparticles uptake in nasal epithelial cells through ligand-receptor interactions, and the damage to nasal tissue since WGA showed cytotoxicity to cells in a dose-dependent manner. In this study, the effect of WGA density on WGA–NP was studied with regard to both the uptake and toxicity *in vitro*, using Calu-3 cells, which express a number of *N*-acetylglucosamine on their cell surface. Nanoparticles containing different WGA ligand densities were prepared by controlling the molar ratio of thiolated WGA to maleimide–PEG–PLA (WGA/maleimide) and particles properties were examined. With the increase of WGA/maleimide ratio, the particle size, WGA density and the hemoagglutination increased, while the conjugation efficiency decreased. The *in vitro* study showed markedly enhanced endocytosis of WGA–NP compared to NP in Calu-3 cells and significant inhibition of uptake in the presence of chitin. Cytotoxicity of WGA–NP increased gradually with the increase of molar ratio of WGA to maleimide, nanoparticles concentration and incubation time. WGA–NP showed the highest efficiency of uptake and a mild cytotoxicity when the molar ratio of WGA to maleimide was 1:10. These results suggest that WGA density plays an important role in both cellular uptake and toxicity of WGA–NP via a receptor-mediated mechanism. Therefore, to achieve a more rational approach of drug delivery system design, the surface density of the targeting moiety on the nanoparticles surface should be considered.

1. Introduction

Intranasal delivery is a noninvasive and convenient method that rapidly targets therapeutics to the central nervous system (CNS), bypassing the blood-brain barrier and minimizing systemic exposure (Dhuria et al., 2010). However, a variety of factors may compromise nasal drug absorption and the access to the brain, especially for peptides and proteins. Firstly, similar to other mucosa, the nasal mucosa provides a substantial barrier to the free diffusion of macromolecular (Donovan et al., 1990). Secondly, enzymatic activities present in nasal secretions can limit protein delivery (Sarkar, 1992). Thirdly, the typical residence time of a protein delivered to the nasal mucosa is only 15–30 min due to rapid ciliary clearance (Schipper et al., 1991).

Previous studies in our group have demonstrated that intranasal administration of peptides encapsulated in wheat germ agglutinin (WGA) modified PEG–PLA nanoparticles (WGA–NP) is a promising approach since nanoparticles cannot only protect macromolecules from peptidase degradation in the nasal milieu, but also improve the delivery of drugs to the brain (Gao et al., 2007). Vasoactive intestinal peptide (VIP; M_W 3326), a neuroprotective peptide, was incorporated into WGA–NP and administered intranasally in rats, and the concentrations of intact VIP were found to increase in the olfactory bulb, cerebrum and cerebellum by 5.66-fold, 6.61-fold and 7.74-fold when compared with intranasal solution, respectively; and about 1.58-fold, 1.82-fold and 1.63-fold compared with unmodified nanoparticles. The increase in VIP concentrations also corresponded to improved memory function, as determined by the water maze behavioral test (Gao et al., 2007). These intriguing results clearly indicated that WGA–NP might serve as a promising

* Corresponding author at: Department of Pharmaceutics, School of Pharmacy, Fudan University, Shanghai 201203, PR China. Tel.: +86 21 51980068; fax: +86 21 51980069.
E-mail address: qzzhang70@yahoo.com.cn (Q. Zhang).

0378-5173/$ – see front matter © 2011 Elsevier B.V. All rights reserved.
doi:10.1016/j.ijpharm.2011.04.026

carrier for intranasal delivery of bio-active molecules, such as peptides and proteins.

WGA, a bioadhesive and non-allergenic lectin, binds to *N*-acetylglucosamine and sialic acid residues both of which are abundant on the nasal epithelial membrane (Ishikawa and Isayama, 1987). Conjugation of WGA on the surface of PEG–PLA nanoparticles (NP) is in favor of prolonging the residence time of NP in nasal cavity and facilitating their internalization (Lehr, 2000). However, the effect of WGA density on binding and cellular uptake of NP by nasal epithelial cells has not been explored. Reports have shown that the cellular uptake often increases with the increase of conjugated ligands on the surface of particles (Yeeprae et al., 2006; Gu et al., 2008; Garg et al., 2009). In general, the ligands must be present above a minimum threshold for binding to occur (Olivier et al., 2003). However, a few studies also showed that dense surface coverage may not offer expected improvements in binding and cellular uptake (Olivier et al., 2003; Gu et al., 2008; Fakhari et al., 2010). These controversial findings require clarification in order to avoid confusion.

Besides the effect of WGA density on cellular uptake, we also hope to know the effect of WGA density on cytotoxicity of WGA–NP, which is associated with the application of WGA–NP for nasal delivery in practice (Mistry et al., 2009). It was reported that WGA can induce apoptosis in cells such as mouse fibroblast cell line L929 and hemopoietic stem cells *in vitro* in a dose-dependent manner (Lustig and Pluznik, 1976; Sun et al., 2001; Reynoso-Camacho et al., 2003). Therefore, determining an optimal WGA conjugation density on NP surface is essential.

During the past twenty years, a few cell models have been developed and used for studies on nasal transport and toxicity (Dimova et al., 2005). Among them, primary-cultured human nasal epithelial cells (HNEC) are generally recognized as a promising system (Audus et al., 1990; Werner and Kissel, 1996; Agu et al., 2003; Mallants et al., 2009), since HNEC retains most features of normal nasal epithelium such as polarity, cilia and mucus secretion. However, this cell model still has its drawbacks: limited resources, sophisticated separation technique, insufficient number of cells from one donor and difficulties in culturing (Dimova et al., 2005). The human lung carcinoma cell line Calu-3 has properties similar to the serous cells of the upper airway (Witschi and Mrsny, 1999). At an air–liquid interface Calu-3 cells grow as a confluent sheet and form polarized monolayers with tight junctions (resulting in a transepithelial electrical resistance of 100–400 $\Omega\,cm^2$), and a uniform mucus layer (Shen et al., 1994; Witschi and Mrsny, 1999; Foster et al., 2000). P-gp, CFTR, several ion channels and a quantity of hydrolase, transferase and cytochrome (Foster et al., 2000; Macvinishl et al., 2007) were also expressed in Calu-3 cell line. And, *N*-acetylglucosamine, an important property for simulating nasal epithelial cells to study the absorption of WGA–NP, was found on the surface of the membrane (Berger et al., 1999). Up to now, Calu-3 cell line has been used as an *in vitro* nasal platform to investigate the microparticles and polymer gels for protein delivery (Witschi and Mrsny, 1999).

The purpose of this study is to optimize WGA density with Calu-3 cell model to evaluate the uptake efficiency and cytotoxicity of WGA–NP. The optimal ligand density was defined as the minimum amount of WGA on the NP surface to offer maximal targeted cellular uptake and mild cytotoxicity. To control the surface density of the targeting protein, WGA–NP was prepared by varying the molar ratio of thiolated WGA to maleimide–PEG–PLA (WGA/maleimide) in this study. A lipophilic fluorescent probe with high sensitivity, 6-coumarin, which was widely used in the *in vitro* and in vivo experiments (Desai et al., 1997; Panyam and Labhasetwar, 2003; Lu et al., 2005; Gao et al., 2007), was incorporated into the NP and used in cellular uptake study.

2. Materials and methods

2.1. Materials

Methoxy poly(ethylene glycol)$_{3000}$-poly(lactic acid)$_{50000}$ (MePEG-PLA) and maleimide- poly(ethylene glycol)$_{3000}$-poly(lactic acid)$_{70000}$ (Male-PEG–PLA) were purchased from University of Electronic Science & Technology of China, Sichuan, China. WGA and Chitin were obtained from Vector Laboratories (UK); 5,5-dithiobis (2-nitrobenzoic acid) (Ellman's reagent), from Acros (Belgium); 6-coumarin from Aldrich. Calu-3 cells were purchased from American Type Culture Collection (ATCC, Manassas, VA, USA). Dulbecco's Modified Eagle Medium/Ham F12 1:1 (DMEM/F12) and fetal bovine serum (FBS) were obtained from Gibco (Invitrogen, USA). Acian blue 8GX was purchased from Amresco (USA), 2-iminothiolane hydrochloride (2-IT), FITC-WGA and 2′,7′-dichlorofluorescin diacetate (DCFH–DA) were purchased from Sigma Chemical Company (USA); Cell counting kit-8 (CCK-8) was obtained from Dojindo Laboratories (Japan). The GSH-400 colorimetric assay kit and LDH assay kit were purchased from Jiancheng Bioengineering Institute (Nanjing, Jiangsu, China). All the other chemicals were analytical reagent grades and used without further purification.

2.2. Preparation of PEG–PLA nanoparticles with different WGA density

PEG–PLA nanoparticles (NP) preparation was based on the emulsion/solvent evaporation technique as previously described with minor modification (Gao et al., 2006). Briefly, MePEG–PLA (22.5 mg) and Male-PEG–PLA (2.5 mg) were dissolved in 1 ml dichloromethane. The polymer mixture was then emulsified by sonication (280 W, 1 min) on ice bath with a probe sonicator (Scientz Biotechnology Co. Ltd., China) in 2 ml of a 1% (w/v) sodium cholate aqueous solution. Immediately after sonication, the o/w emulsion obtained was diluted into 20 ml of a 0.5% (w/v) sodium cholate aqueous solution under magnetic stirring for 5 min. After dichloromethane evaporation, the NP were collected by centrifugation and then resuspended in 0.5 ml of a 0.05 M HEPES buffer pH 7.0 adding 0.15 M NaCl for further use. 6-coumarin loaded NP were prepared with the same procedure except that 0.005% (w/v) of 6-coumarin was added to the dichloromethane solution before emulsification and the obtained NP were subjected to a 1.5 × 20 cm sepharose CL-4B column and eluted with 0.05 M HEPES buffer pH 7.0 adding 0.15 M NaCl to remove the unentrapped 6-coumarin.

WGA was thiolated for 60 min with a 1:60 molar ratio of WGA to 2-iminothiolane. The product was purified using Hitrap™ Desalting column (GE Healthcare, USA), with the protein fractions collected. The thiolated WGA was conjugated with NP at a WGA/maleimide molar ratio of 1:50, 1:25, 1:10, 1:3, 1:1 and 2:1. The reaction was performed at room temperature for 8 h. Unconjugated WGA was removed by centrifugation and nanoparticles obtained were then washed 3 times with Milli-Q treated water.

2.3. Characterization of nanoparticles

2.3.1. Morphology, particle size and zeta potential

Mean (volume-weighted) diameter and zeta potential of the nanoparticles were determined by dynamic light scattering (DLS) using Zeta Potential/Particle Sizer Nicomp 380 ZLS (Particle Sizing Systems, Santa Barbara, USA). The morphology of nanoparticles was observed under a transmission electron microscope (H-600, Hitachi, Japan) following negative staining with sodium phosphotungstate solution.

2.3.2. Determination of conjugation density

In order to determine the lectin density at the surface of the resulting particles, the concentration of unconjugated WGA after centrifugation and wash procedure (Section 2.2) was measure with ELISA method. The WGA–NP concentration was determined by turbidimetry using UV2401spectrophotometer at 350 nm (Shimadzu, Japan). The conjugation density and efficiency were calculated as indicated below.

$$\text{Conjugation density} = \frac{(\text{amount of WGA added} - \text{amount of unconjugated WGA})}{\text{total amount of nanoparticles}}$$

$$\text{Conjugation efficiency} = \frac{(\text{amount of WGA added} - \text{amount of unconjugated WGA})}{\text{amount of WGA added}} \times 100\%$$

2.3.3. Haemagglutination test

The influence of WGA density on the bioactivity of WGA–NP was assessed by WGA-induced haemagglutination test. 200 μl of WGA–NP (0.5 mg/ml) at a WGA/maleimide molar ratio of 1:25, 1:10 and 1:3 were respectively incubated with 200 μl 10% (v/v) suspension of fresh rat erythrocyte in PBS (pH7.4) at 37 °C for 30 min. The erythroagglutination of each group was observed by a light microscope (UFX-DX, Nikon, Japan) at enlargements of 400×. Unmodified NP was used as a negative control. The procedure was conducted in triplicate.

2.3.4. Determination of the encapsulation efficiency and loading capacity

The loaded amount of 6-coumarin in WGA–NP and NP were detected using HPLC (Davda and Labhasetwar, 2002). A predetermined amount of WGA–NP and NP were dissolved in three-fold volumes of acetonitrile, and further diluted with methanol. Then 20 μl of the diluted sample was injected into the Agilent 1200 HPLC system (Agilent Technologies, USA) consisting of a Quat Pump (Model G1311A) and a fluorescence detector (Model G1231A; ex = 465 nm, em = 502 nm). With the Dikma Diamonsil®C_{18} (5 μm, 200 mm × 4.6 mm) column, the separations were achieved using methanol and water at the ratio of 96:4 as the mobile phase with a flow rate of 1.2 ml/min and column temperature at 35 °C. The 6-coumarin loading capacity (DLC) and encapsulation efficiency (EE) was calculated as follow:

$$\text{EE}(\%) = \frac{C \times V}{T} \times 100\% \quad \text{DLC}(\%) = \frac{C \times V}{M \times 1000} \times 100\%$$

Where C indicates the concentration of 6-coumarin encapsulated in the nanoparticles, V represents the volume of diluted nanoparticle solution, M denotes the total weight of the nanoparticles and T represents the amount of 6-coumarin added.

2.3.5. In vitro release study of 6-coumarin from WGA–NP

In vitro release of 6-coumarin from the nanoparticles were performed by incubating 6-coumarin-loaded WGA–NP and NP at a nanoparticles concentration of 60 μg/ml at 37 °C in pH 4.0 and pH 7.4 PBS, which represented the pH in the endo-lysosomal compartment and physiologic pH, respectively. Samples (n = 3) were withdrawn at predetermined time and subject to centrifugation at 21,000 g for 45 min, the supernatant was further diluted with one-fold volume of methanol and analyzed for the released amount of 6-coumarin by HPLC assay. Furthermore, in order to reduce the influence of time-related quenching of the fluorescence, three additional samples were simultaneously taken for the determination of the total amount of fluorescence retained in the samples at each time point using HPLC analysis method described in Section 2.3.4. The cumulative release percentage of 6-coumarin from nanoparticles at each time point was calculated by dividing the amount of 6-coumarin in supernatant by total amount of 6-coumarin.

2.4. Cell culture and characterization

Calu-3 cells were maintained in 10 cm tissue culture dishes in Dulbecco's Modified Eagle Medium/Nutrient Mixture F-12 (DMEM/F12 1:1) medium supplemented with 10% fetal bovine serum, 1% non-essential amino acids, penicillin (100 U/ml) and streptomycin (100 mg/ml). Each week, cells were passaged and seeded onto rat tail collagen coated (30 mg/mL) Transwell filters at a density of 5×10^5 cells/cm^2, and cultured in a humidified atmosphere of 5% CO_2/95% air at 37 °C. After 48 h, an air-interface was created and the cells were maintained with 0.6 mL of culture medium in the basolateral chambers of Transwells. The air-interface conditions stimulated differentiation of the cell monolayer to form polarized, bioelectrically "tight" epithelial monolayer. The passages used for the following experiments were 30–40. Transepithelial electrical resistance (TEER) values were measured with a Millicell ERS (Millipore, MA, USA) and the morphology of cell monolayer were observed using transmission electron microscope (PHILIPS CM-120, Holland).

Alcian blue staining, which is commonly used to detect mucus expression, was used to investigate the acidic mucin on the cell surface. Cell layers were washed twice with PBS (pH 7.4) and fixed with 4% paraformaldehyde. Then the cells were washed again with PBS and stained with 1% (w/v) alcian blue in a solution of 3% (v/v) acetic acid (pH 2.5) for 1 h at 37 °C. The dye was then removed and cell layer washed with PBS until the rinsate ran clear.

To demonstrate that the cell line expressed *N*-acetylglucosamine, an important property for simulating nasal epithelial cells to study the cellular uptake of WGA–NP, lectin staining was conducted as follow: Calu-3 cells were seeded on polylysine-coated coverslips at a density of 1.0×10^5 cell/cm^2. After culture for 24–48 h, coverslips containing Calu-3 cells were rinsed in PBS and preincubated with neuraminidase (1 IU/ml) at 37 °C for 30 min to remove the sialic acid residues on the membrane surface. Then the cells were washed with PBS and fixed with 4% paraformaldehyde for 20 min. Cells were treated with FITC labeled WGA solution (0.1 mg/ml) for 30 min at 37 °C, rinsed with PBS for 3 times, mounted using Mowiol and observed under fluorescent microscope (Olympus, Japan)

2.5. Cellular uptake of WGA–NP and NP

2.5.1. In vitro uptake study

Calu-3 cells were seeded in 24-well plates at a density of 1×10^5 cells/cm^2 and grew for 24–36 h. After pre-incubation with HBSS for 15 min, the medium was replaced with the suspension of 6-coumarin-loaded nanoparticles (prepared in HBSS) and incubated at 37 °C. Uptake was terminated by washing the cells with ice-cold PBS (pH 7.4) for five times. Subsequently, the cells of each well were solubilized in 400 μl 1% Triton X-100 and 25 μl of the cell lysates were used to measure the total cell protein content using BCA protein assay (Shanghai Shenergy Biocolor Bioscience and Technology Co., Ltd., China). Another 100 μl of the cell lysates were lyophilized, extracted 6-coumarin with methanol and used for HPLC analysis to quantify nanoparticles. The determination method was the same as described in Section 2.3.4. A calibration curve for nanoparticles was constructed by suspending different concentrations of nanoparticles (5–250 μg/ml) in 1% Triton X-100 followed by lyophilization and extraction of 6-coumarin. The uptake of nanoparticles by Calu-3 cells was calculated with the calibration curve and expressed as the amount (mg) of nanoparticles uptaken per mg cell protein.

The effects of WGA density, nanoparticles concentration, incubation time, temperature and sugar receptor inhibitor on cellular uptake were determined in present study. (i) To examine the effect of the WGA density on NP surface for efficient targeting to Calu-3 cells, WGA–NP prepared with different WGA/maleimide molar ratios (1:50, 1:25, 1:10, 1:3, 1:1 and 2:1) and NP at the concentration of 500 μg/ml were incubated with cells at 37 °C for 2 h, respectively. The optimal ratio for uptake was chosen in the subsequent experiment. (ii) To evaluate the effect of different concentrations of WGA–NP on the uptake, Calu-3 cells were incubated with WGA–NP in the concentration range of 0.1–5 mg/ml for 2 h at 37 °C. (iii) To investigate time-dependent uptake, cells were incubated with 1 ml suspension of WGA–NP (500 μg/ml) for 0.25, 0.5, 1, 2 and 4 h at 37 °C. (iv) To study the effect of incubation temperature on cellular uptake, cells were incubated for 2 h with three different nanoparticle concentrations (0.2, 0.5 and 1 mg/ml) at both 37 °C and 4 °C. (v) To confirm that the cellular uptake of WGA–NP was via *N*-acetylglucosamine receptor-mediated mechanism, a sugar receptor inhibitor-chitin (0.6 mg) was preincubated with WGA–NP (0.5 mg) at 37 °C for 3 h in 0.01 M HEPES buffer (pH 8.5) adding 0.1 mM $CaCl_2$. Then the mixtures (containing 500 μg/ml WGA–NP) were incubated with Calu-3 cells for 2 h.

2.5.2. Confocal laser scanning microscopy

Calu-3 cells were seeded onto glass cover slips at 1×10^4 cells/cm^2 for 2 days. The cells were then incubated with 6-coumarin-loaded WGA–NP (1:10) or NP suspensions (500 μg/ml in HBSS) for 15, 30 and 120 min at 37 °C, respectively. After incubation period, the supernatants were removed. Cells were then washed three times with ice-cold PBS (pH 7.4) to remove adhering nanoparticles and fixed with 4% paraformaldehyde. Samples were finally embedded in PBS/glycerol (2:1) and examined under confocal laser scanning microscope (Leica TCS SP2 AOBS, Germany).

2.6. Cytotoxicity of nanoparticles

2.6.1. Cell viability assay

To evaluate the cytotoxicity of WGA–NP and NP, cell viability was determined by CCK-8 assay. Calu-3 cells were seeded into a 96-well plate at a density of 5×10^4 cells per well. On the second day, the medium was replaced with 100 μl NP and WGA–NP (1:25, 1:10 and 1:3) suspensions at a concentration of 0.5, 3.125, 12.5 and 50 mg/ml in HBSS. After 4-hour, 24-hour and 48-hour exposure, the cells were incubated in 100 μl fresh culture medium adding 10 μl of CCK-8 solution. After 2-hour incubation, the absorbance of wells was measured using a Microplate Reader (Thermo MULTISKAN MK3, USA) at 450 nm and then converted into cell viability according to the instruction provided by manufacturer.

2.6.2. Release of lactate dehydrogenase (LDH)

The LDH test was performed using a commercial LDH assay kit (Jiancheng Bioengineering Institute, China) to monitor the cell membrane damage (Kroll et al., 2009). Calu-3 cells were seeded into a 96-well plate at a density of 5×10^4 cells per well. After 24-hour exposure to NP and WGA–NP (1:25, 1:10 and 1:3) at different concentrations mentioned above, 100 μl of the cell culture supernatants were withdrawn. LDH activity was then determined and calculated according to the manufacturer's protocol (Wang et al., 2010).

2.6.3. Measurement of intracellular reactive oxygen species (ROS)

The production of intracellular ROS was measured using 2, 7-dichlorohydrofluoroscein diacetate (H_2DCF-DA) (Yang et al., 2009). Briefly, cells were seeded into a 24-well plate with 1×10^5 cells per well. After 24-hour exposure to nanoparticles with different concentrations and WGA conjugation density (see Section 2.6.1), the cells were washed twice with PBS and then incubated in 1 ml of 10 μM H_2DCF-DA diluted in HBSS at 37 °C for 30 min. Then cells were washed with PBS and lysed with 200 μl of 0.5% Triton X-100. The fluorescence of dichlorofluoroscein (DCF), the oxidized product of H_2DCF-DA, was measured using the luminescence spectrofluorometer (LS55, Perkin Elmer, USA) with excitation and emission wavelengths of 485 nm and 525 nm, respectively. Intracellular ROS percentage was calculated and expressed as the percentage of control.

2.6.4. Measurement of intracellular reduced glutathione (GSH)

Cellular levels of reduced GSH were determined using the GSH-400 colorimetric assay kit (Jiancheng Bioengineering Institute, China). Calu-3 cells were seeded into a 24-well plate at a density of 1×10^5 cells/well for 24 h, cells were then treated with nanoparticles at different concentrations and WGA conjugation density (see Section 2.6.1) for 24 h. Subsequently, the cells were rinsed three times in ice-cold PBS, homogenized in 500 μl of 0.5% Triton X-100 and centrifuged at 3000 *g* at 4 °C for 10 min. The assay was performed on 400 μl centrifugation supernatants according to manufacturer's protocol, and the absorbance was measured at 405 nm. Protein content was also determined using the same cell homogenate. GSH level was calculated from the absorbance at 405 nm and expressed as the percentage of control.

2.7. Statistical analysis

All the data were expressed as mean ± standard deviation and comparison between different groups was performed by one-way ANOVA followed by Student Newman Keuls post-hoc tests. Differences were considered statistically significant at $p < 0.05$.

3. Results and discussion

3.1. Characterization of NP and WGA–NP

The resulting NP exhibited spherical shape under the examination of a transmission electron microscope with a volume based diameter of 88.9 ± 1.8 nm which increased to more than 94 nm after WGA conjugation (Table 1). A trend of slightly increasing WGA–NP size with increasing WGA/maleimide molar ratio was observed. For example, WGA–NP sizes increased from 94.71 ± 6.52 nm to 116.42 ± 13.79 nm when the ratio of WGA to maleimide increased from 1:50 to 1:1. However, the ratio of 2:1 caused a prominent increase of WGA–NP size (170.96 ± 13.70 nm). The larger particle size was probably due to agglomeration of the particles or crosslink of the thiolated protein (Weissenböck et al., 2004). In present study, the mean particle sizes of WGA–NP with different WGA/maleimide molar ratio were less than 200 nm (Table 1), which is advantageous for nasal mucosa transport. Vila et al. (2005) showed that the efficacy of ^{125}I-TT transport across the nasal mucosa was related to the particle size, reaching the greatest transport for the smallest particle size (196 ± 20 nm). A slight decrease in zeta potential values was observed when WGA/maleimide molar ratio increased, with no significant difference.

WGA was conjugated to NP by connecting thiol groups of the peptide to amine groups on the NP surface. As expected, increasing amount of thiolated lectin resulted in the increase in WGA density. However, the conjugation efficiency, an index to evaluate the availability of the lectin added, decreased (Table 1). When ratio of WGA to maleimide is below 1:3, conjugation efficiency of modified NP is higher than 60%.

And, hemoagglutination test showed that WGA, treated through the covalent coupling procedure, still retained the bioactivity of

Table 1
Characteristics of NP and WGA–NP (mean ± SD, $n = 3$).

	The ratio of thiolated WGA to Maleimide-PEG-PLA	Particle size (nm)	Zeta pontential (mV)	WGA per nanoparticle (μg/mg)	Conjugation efficiency (%)
NP	–	88.9 ± 1.8	−22.17 ± 1.32	–	–
WGA–NP	1:50	94.71 ± 6.52	−21.69 ± 1.54	1.17 ± 0.24	86.27 ± 4.92
	1:25	101.87 ± 5.71	−20.87 ± 1.74	2.29 ± 0.33	84.78 ± 5.74
	1:10	109.92 ± 7.44	−19.43 ± 0.42	5.86 ± 0.26	85.73 ± 7.42
	1:3	115.70 ± 5.30	−18.68 ± 1.20	13.92 ± 0.57	60.83 ± 8.20
	1:1	116.42 ± 13.79	−18.87 ± 1.80	21.20 ± 1.99	41.22 ± 3.88
	2:1	170.96 ± 13.70	−18.23 ± 0.71	49.28 ± 5.33	36.16 ± 3.71

agglutinating red blood cells on the surface of NP (Fig. 1). Furthermore, the hemoagglutination was enhanced with the increase of WGA/maleimide molar ratio, suggesting more WGA was bound to the surface of NP.

Considering the possible receptor/vector saturation of cellular uptake, Calu-3 cell model was used for further optimization of the WGA/maleimide molar ratio.

Incorporation of the fluorescent dye 6-coumarin had no impact on the characteristics of particle. The diameter was 91.2 ± 1.8 nm for NP, 105.5 ± 5.3 nm for WGA–NP (the ratio in this section was 1:10), respectively. Zeta potential values of both NP and WGA–NP were about −28 mV. The DLC% was 0.14 ± 0.01% and 0.12 ± 0.001%, and EE% was 75.75 ± 1.22% and 68.50 ± 0.45% for 6-coumarin-loaded NP and WGA–NP, respectively.

The results of the *in vitro* release study conducted in pH 4.0 and 7.4 PBS at 37 °C, consistent with previous studies (Desai et al., 1997), showed that only 2.63 ± 0.05% (NP, pH 4.0), 3.21 ± 0.37% (NP, pH 7.4), 4.56 ± 0.94% (WGA–NP, pH 4.0) and 3.43 ± 0.47% (WGA–NP, pH 7.4) of 6-coumarin was released from NP and WGA–NP, respectively, even after 24-hour incubation period. These data clearly suggested that almost all the fluorescent dye remained associated with the nanoparticles during the experimental period. Therefore, the fluorescent activity measured in the Calu-3 cells was mainly due to the uptake of nanoparticles.

3.2. Cells characterization

Calu-3 monolayers generally consisted of cuboidal and polygonal cells, which were closely apposed (Fig. 2C). Transmission electron micrographs of Calu-3 monolayers revealed microvilli on the apical surface and electron dense areas near the upper portions of the intercellular junctions where tight junctions would be expected (Fig. 2A, B). The TEER was also used as a measure of monolayer 'tightness'. The resistance values appeared to increase with days in culture until a plateau of 300–400 Ω cm^2 was reached (day 10–14). The results were similar to the previous report (Foster et al., 2000), indicating Calu-3 cells had formed a confluent sheet.

The cell layers were stained with alcian blue, there was prominent blue staining (data not shown), suggesting glycoprotein (mucus) presented covering the cell surface. After digestion of sialic acids and staining with FITC-labeled WGA, Calu-3 cells exhibited green fluorescence widespread on the membrane which indicated high expression of *N*-acetylglucosamine, one of the WGA specific receptors, on the cell membrane (Fig. 2D). The results also proved the potential for the Calu-3 cell line as a useful tool to evaluate WGA–NP absorption via nasal route.

3.3. In vitro uptake study

3.3.1. Uptake conditions study

In order to define the uptake characteristics of WGA–NP, the uptake conditions were studied in term of nanoparticles concentration, incubation time and temperature. Uptake of WGA–NP by the Calu-3 cells at 37 °C was seen at as early as 15 min and increased rapidly within the initial 2 h after incubation. The time-dependent uptake overall increased linearly ($R^2 > 0.97$) with the incubation time up to 4 h (Fig. 3A). The uptake of WGA–NP in Calu-3 cell was also dependent on the concentration of nanoparticles in the range of 0.1–1 mg/ml (Fig. 3B). However, further increase in concentration to 5 mg/ml showed no significant increase in cell uptake, indicating a saturation limit. When the incubation temperature was reduced to 4 °C, the uptake of the nanoparticles (1 mg/ml) decreased by 74.5% for NP and 50% for WGA–NP when compared to uptake at 37 °C (Fig. 3C), suggesting the temperature dependence of uptake. At 4 °C, cellular uptake of WGA–NP increased 8.7 folds when nanoparticles concentration increased from 0.2 mg/ml to 1 mg/ml, obviously higher than a 3.5-fold increase of NP, indicating that the uptake of WGA–NP was less dependent on energy than that of NP (Legen et al., 2003). These results demonstrated that Calu-3 cells uptake of WGA–NP was concentration- and energy-dependent, suggesting an active transport process.

3.3.2. Uptake inhibition study

To verify the uptake mechanism of WGA–NP in a *N*-acetylglucosamine receptor-mediated manner, competitive uptake experiments on WGA–NP were performed with or without an excess of chitin (a long-chain polymer of a *N*-acetylglucosamine). It was found that preincubation with excess chitin significantly reduced the uptake efficiency of WGA–NP to 37% (Fig. 3D), demonstrating that WGA bound to the specific receptors on the membrane and then resulted in the cellular uptake of WGA–NP. Since the efficient uptake through a receptor-mediated mechanism is largely

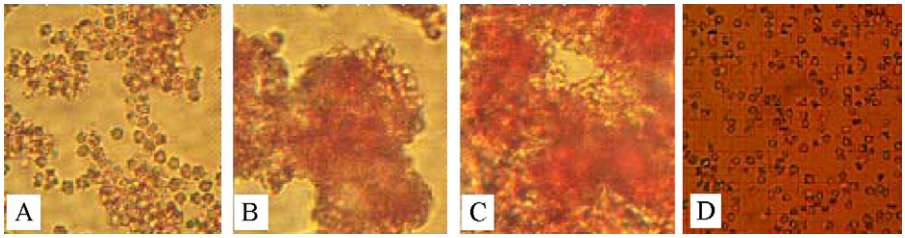

Fig. 1. Images of erythrocytes under microscope after incubation at 37 °C for 30 min with 0.5 mg/mL WGA–NP at WGA/maleimide molar ratio of 1:25 (A), 1:10 (B), 1:3 (C), respectively. (400×). The hemoagglutination was enhanced with the increase of WGA/maleimide molar ratio, while unmodified NP did not show the bioactivity of agglutinating red blood cells (D).

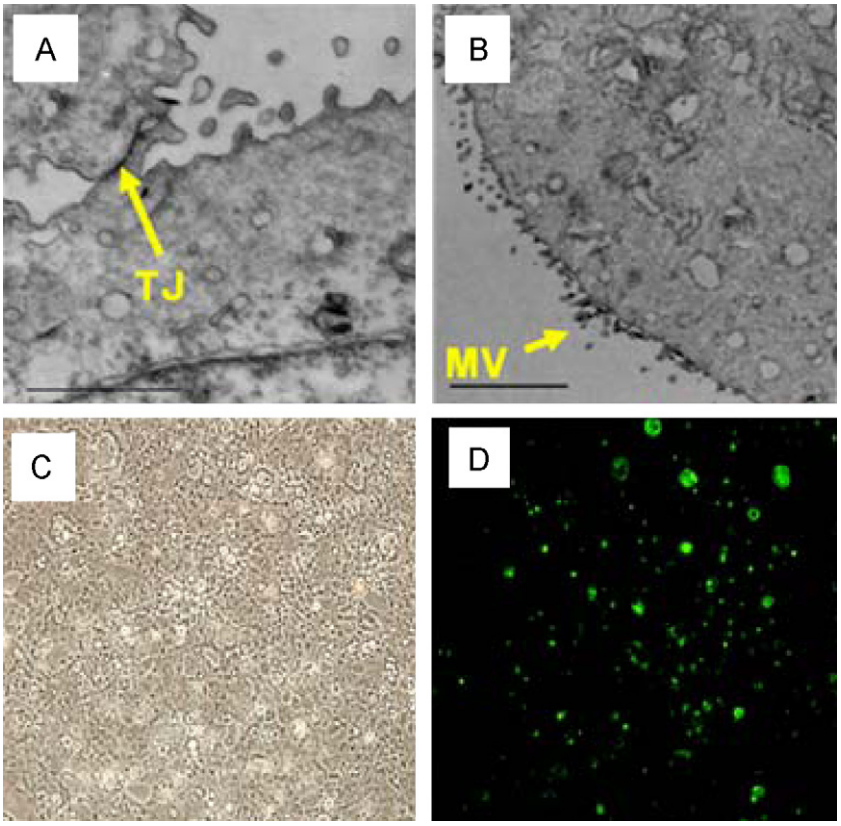

Fig. 2. TEM images of Calu-3 cells at day 14 with (A) tight junction (TJ) and (B) short microvilli (MV). (A) Scale bar = 1 μm, (B) scale bar = 2 μm; (D) FITC-WGA staining of Calu-3 cells treated with neuraminidase prior to WGA staining (100×, right), (C) is the corresponding phase contrast image.

controlled by ligand-receptor interaction, the results of inhibition experiments of chitin prompted us to investigate the effect of WGA density on the cellular uptake of WGA–NP to achieve a more rational approach to the design of drug delivery systems.

3.3.3. The effect of WGA density on cellular uptake of 6-coumarin-loaded WGA–NP

As shown in Fig. 4, when the WGA/maleimide molar ratio was 1:50, WGA–NP showed no significant increase in uptake compared

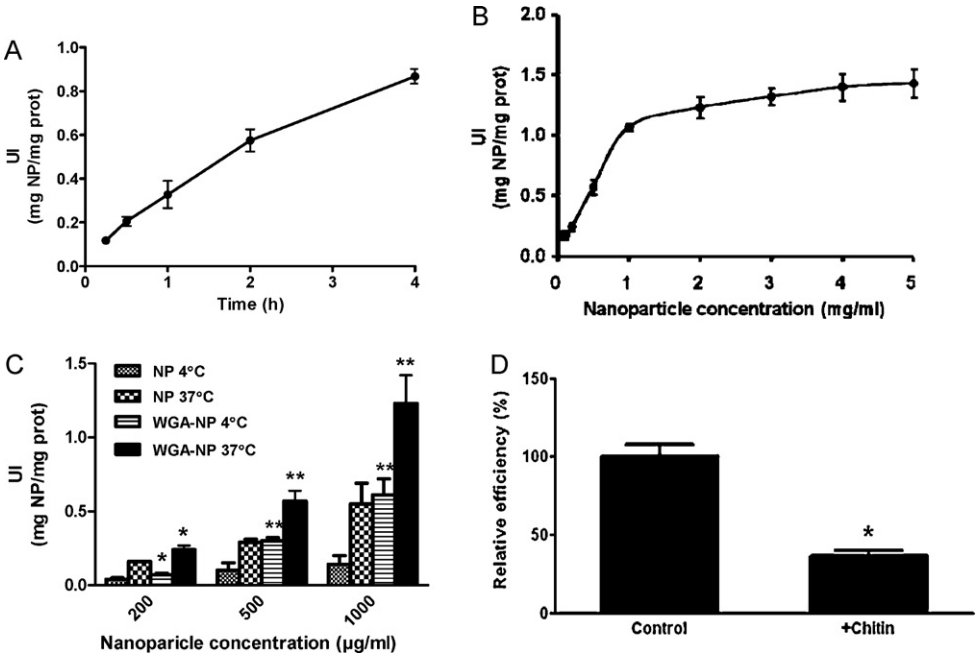

Fig. 3. (A) The effect of incubation time on uptake of WGA–NP by Calu-3 cells, cells were incubated with 500 μg/ml nanoparticles at 37 °C; (B) The effect of concentration on uptake of WGA–NP by Calu-3 cells at 37 °C for 2 h; (C) Calu-3 uptake NP and WGA–NP at 37 °C and 4 °C respectively for 2 h; (D) Relative uptake efficiency of 500 μg/ml WGA–NP by Calu-3 cells at 37 °C when treating with sugar receptor inhibitor. The cellular uptake without any inhibition was used as controls. Data are mean ± SD, $n = 4$, $^{*}p < 0.01$ $^{**}p < 0.001$ versus NP group.

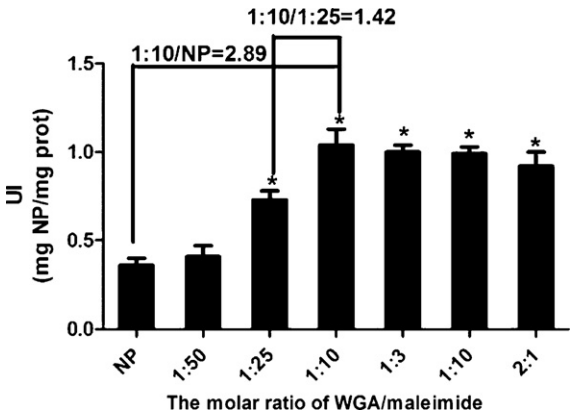

Fig. 4. Calu-3 uptake 500 μg/mL NP and WGA–NP with different amount of conjugated WGA at 37 °C for 2 h (mean ± S.D., $n = 4$). *$p < 0.01$ versus NP group.

to NP ($p > 0.05$). The maximum uptake, about 2.89 times higher than that of NP, was achieved at the WGA/maleimide molar ratio of 1:10, which was significantly higher than that of 1:50 and 1:25 groups (about 2.39 times and 1.42 times, respectively). With further increase in WGA/maleimide molar ratio from 1:10 to 2:1, a slight decrease but no significant difference was observed on cellular uptake of WGA–NP ($p > 0.05$). This was possibly caused by the saturation of WGA-receptor on cells when the ratio reached 1:10. Similar results were reported by Fakhari et al. (2010), who found the optimal surface density of cLABL peptide on PLGA NPs was about 2–4 pmol/cm^2. Interestingly, the minimum uptake for PLGA NPs occurred in the maximum peptide density.

For WGA conjugated PEG–PLA nanoparticles, the PEG on NP surface provides a steric barrier allowing the NP to circulate in the blood and the functionalizing moiety, WGA peptide, will specifically recognize and bind to *N*-acetylglucosamine expressing cells. Though high peptide density is assumed to increase NP binding to cell receptors, however, excess WGA will mask PEG on NP surface, thus diminish NP stealth properties in vivo. Gu et al. (2008) found increasing A10 aptamer (Apt) density, which binds to the prostate-specific membrane antigen on the surface of prostate cancer cells, inversely affected the amount of PEG exposure on NP surface and identified the narrow range of Apt density when the NP were maximally targeted and maximally stealth. In this case, the optimum density of WGA may be about 5.8–21 μg/mg NP (Table 1).

In our previous study, WGA–NP prepared at the ratio of thiolated lectin to maleimide of 1:3 enhanced the brain delivery of VIP following intranasal administration (Gao et al., 2007). Nevertheless, a comparable cellular uptake was found when WGA/maleimide molar ratio reduced to 1:10 in this study. Due to a lower lectin usage amount, the ratio of 1:10 will be favorable for WGA–NP application as a carrier in the case of cost and toxicity.

3.3.4. Confocal microscopy study

Confocal microscopy was further conducted to visualize the cellular uptake of NP and WGA–NP (at molar ratio of 1:10). Calu-3 cells were incubated with NP and WGA–NP at the same concentration (500 μg/mL) for 15, 30 and 120 min at 37 °C, respectively. The images demonstrated that the increase of fluorescent intensity in the cells was correlated with the increase of incubation time (Fig. 5). The obvious uptake of WGA–NP was observed only after 15 min. There was a significantly accumulated amount of WGA–NP in the cells compared with that of NP at each time point, suggesting that uptake of WGA–NP was more rapidly and effectively than that of NP. The data were consistent with the results shown by the quantative analysis (2.89 times higher uptake of WGA–NP in Calu-3 cells than that of NP after 2-hour incubation).

3.4. Cytotoxicity of NP and WGA–NP

3.4.1. Cell viability

In this section we selected nanoparticles prepared at three WGA/maleimide molar ratio (1:25, 1:10, 1:3) for further investigation of cytotoxicity, which displayed less aggregation and higher conjugation efficiency than that of 2:1 and 1:1 molar ratio.

The viability of Calu-3 cells incubated with NP and WGA–NP were shown in Table 2. The viability of cells decreased with the increase of nanoparticles concentration, incubation time and WGA/maleimide molar ratio. Unmodified nanoparticles did not show significant cytotoxicity at any concentration and incubation time. WGA–NP with molar ratio of 1:25 also had no distinct toxicity, displaying more than 80% viability even after 48-hour incubation. WGA–NP with molar ratio of 1:10 and 1:3 presented no toxic or mild toxic on cells at the concentration below 12.5 mg/ml, respectively. But when the concentration increased to 50 mg/ml, the cell

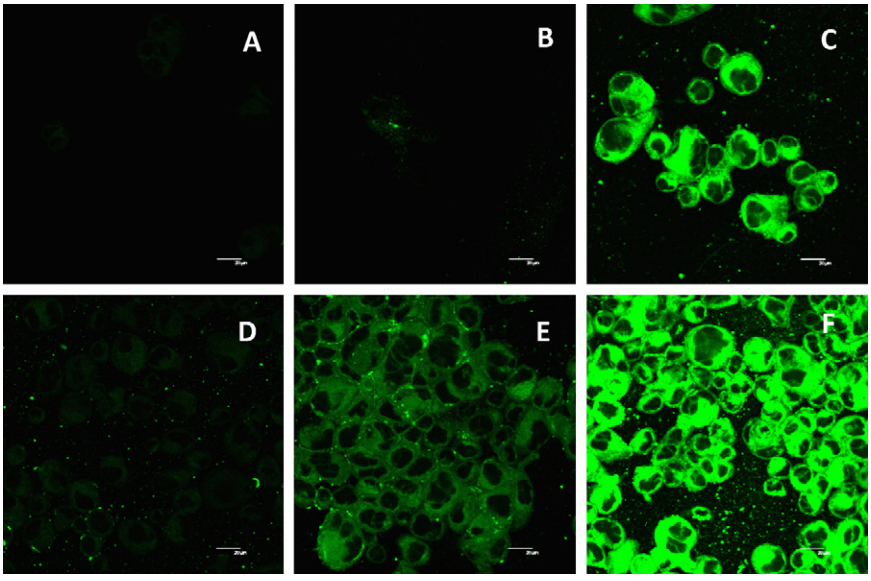

Fig. 5. Calu-3 uptake 500 μg/ml NP and WGA–NP at 37 °C for 15 min (A, D), 30 min (B, E) and 120 min (C, F), respectively. The bar on each photo is 20 μm.

Table 2
The viability of Calu-3 cells after exposure to NP and WGA–NP ($n = 3$).

	Dosage (mg/ml)	Viability (%)		
		4 h	24 h	48 h
NP	0.5	100.22 ± 7.09	100.48 ± 8.95	99.66 ± 7.95
	3.125	97.85 ± 8.63	97.49 ± 2.95	97.20 ± 12.56
	12.5	97.45 ± 3.79	97.35 ± 2.93	90.67 ± 3.42
	50	98.18 ± 11.13	96.03 ± 7.95	91.39 ± 0.95
WGA–NP (1:25)	0.5	101.96 ± 1.71	109.27 ± 3.76	103.71 ± 3.30
	3.125	99.64 ± 5.89	94.53 ± 5.06$^{\#}$	101.45 ± 0.61
	12.5	99.65 ± 3.19	84.20 ± 1.93$^{*,\#}$	93.24 ± 3.83
	50	92.51 ± 8.02	83.95 ± 2.08$^{*,\#}$	80.52 ± 2.59$^{*,\#}$
WGA–NP (1:10)	0.5	101.74 ± 1.71	109.69 ± 4.03	101.67 ± 3.03
	3.125	102.48 ± 3.85	100.36 ± 0.82	101.84 ± 1.98
	12.5	96.18 ± 3.23	83.06 ± 1.97*	81.31 ± 3.18$^{*,\#}$
	50	82.67 ± 3.08$^{*,\#}$	73.85 ± 1.88$^{*,\#}$	66.13 ± 7.25$^{*,\#}$
WGA–NP (1:3)	0.5	101.04 ± 4.02	108.42 ± 3.83	100.68 ± 12.74
	3.125	97.67 ± 2.83	101.60 ± 6.09	102.00 ± 0.28
	12.5	90.22 ± 6.65	81.52 ± 4.67$^{*,\#}$	79.45 ± 4.87$^{*,\#}$
	50	68.57 ± 1.72$^{*,\#}$	61.83 ± 4.00$^{*,\#}$	55.43 ± 4.86$^{*,\#}$

* $p < 0.05$ versus control (The control used was the cells cultured in the medium without any additional solutions).
$^{\#}$ $p < 0.05$ versus NP group.

viability was reduced to 74% for 1:10, and 61% for 1:3 after 24 h incubation. Cell viability of 48-hour incubation was similar to that of 24-hour. In a word, cell viability values were all more than 50% within the concentration range from 0.5 to 50 mg/ml. According to the United States Pharmacopoeia (U S Pharmacopeia XXXII, 2009) Biological Reactivity Test *in vitro*, cell relative proliferation rate (RPR) more than 50% indicated mild cytotoxicity of biomaterial, so the present results proved WGA–NP to be a safe carrier *in vitro*.

3.4.2. LDH leakage

Cell membrane disruption was reflected in the elevated LDH levels in the cell medium after cells were exposed to nanoparticles (Lin et al., 2006). In present study, LDH levels in cell medium were dependent on nanoparticle concentrations and WGA/maleimide molar ratio (Fig. 6). NP only at a concentration of 50 mg/ml resulted in significantly elevated LDH level in the cell medium ($p < 0.05$), suggesting NP had weak membrane damage on Calu-3 cells. While three WGA–NP groups remarkably increased LDH levels released in cell supernatant, especially for 1:3 group. For example, following exposure to WGA–NP 1:3 in the range of 0.5–50 mg/ml, LDH releases were increased by 107.5–156.5%, significantly higher than the untreated control ($p < 0.05$), suggesting that WGA coupling with NP damage the cell membrane integrity.

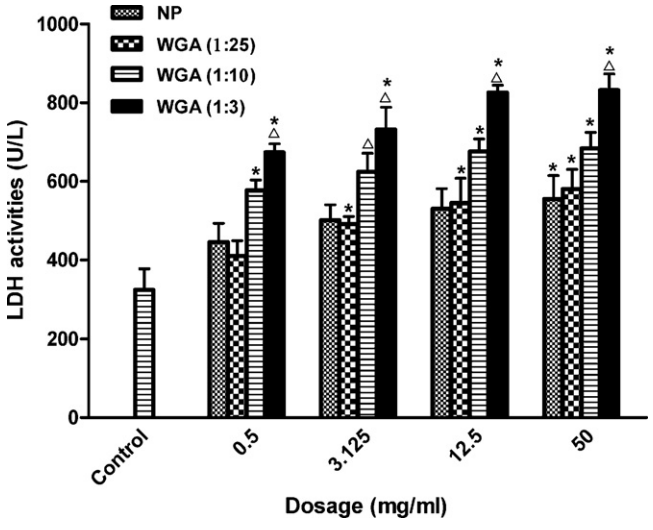

Fig. 6. The LDH level in culture medium after 24-hour exposure to NP and WGA–NP. Data are mean ± SD, $n = 3$, $^{*}p < 0.05$ versus control cells; $\Delta p < 0.05$ versus NP group.

3.4.3. ROS and GSH

GSH is a ubiquitous thiol-containing molecule in cells that is responsible for maintaining cellular oxidation–reduction homeostasis (Cecarini et al., 2007). The mitochondria bring out the reactive oxygen species (ROS) during ATP production. Various ROS, such as superoxide, hydrogen peroxide, hydroxyl and other oxygen radicals, are involved in oxidative stress and cells will be damaged with excessive generation of ROS (Kroll et al., 2009). Therefore, alterations in GSH homeostasis and intracellular ROS level can be considered as indication of functional damage to the cells.

Nanoparticles decreased GSH levels in the cells in dose- and WGA/maleimide molar ratio dependent manner (Fig. 7A). There was slight decrease of GSH but no significant difference among NP, WGA–NP of 1:25 and 1:10 groups at almost all the concentrations above-mentioned except for 50 mg/ml ($p < 0.05$). However, WGA–NP 1:3 group at each concentration resulted in a sharp drop of GSH level, the intracellular GSH was reduced by about 30% when the concentration increased from 0.5 to 12.5 mg/ml, and reduced by 70% at 50 mg/ml compared with the control.

In contrast, the changes in ROS level were less apparent than that in GSH (Fig. 7B). Compared with the control, WGA–NP of 1:10 and 1:3 groups only at 12.5 and 50 mg/ml showed slightly increase of ROS ($p < 0.05$). Taken together, the data revealed that WGA–NP at high concentration and high WGA/maleimide molar ratio cause damage to Calu-3 cells. The cytotoxicity is ranked as: WGA–NP (1:3) > WGA–NP (1:10) > WGA–NP (1:25) > NP.

As an ectogenic agglutinin, WGA was reported to induce apoptosis in pancreatic cancer cells *in vitro* (Schwarz et al., 1999). The necessary steps that WGA induce toxicity appear to involve WGA binding to sialic acid residues of glycoprotein on cell surface, cellular uptake and subsequent localization to the nucleus (Schwarz et al., 1999; Sun et al., 2001). Our results indicating that the cellular uptake of WGA–NP might be enhanced with the increase of dosage and the higher WGA density on NP surface. Upon endocytosis, WGA–NP with higher WGA density showed higher affinity to *N*-acetylglucosamine on the nucleus membrane, which resulted in more particles locating to the perinuclear region, thus inducing more severe oxidative damage to the cells. LDH leakage from cells is another evidence for penetration of particles into the cells and damage of cell membrane.

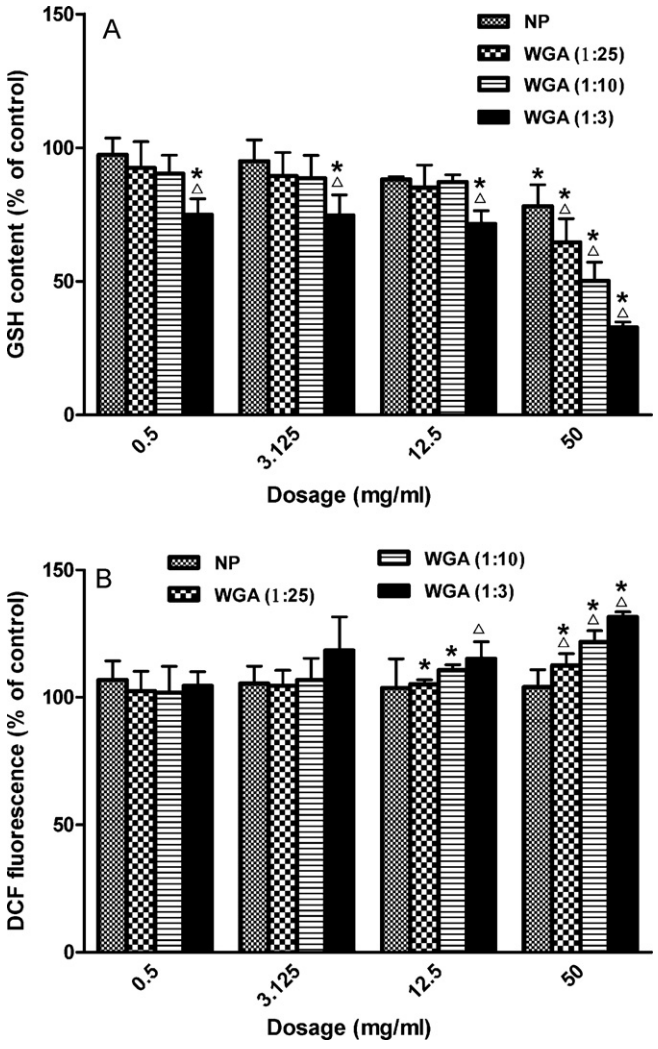

Fig. 7. Effect of nanoparticles on (A) GSH levels (B) ROS generation in Calu-3 cells. Cells were exposed to nanoparticles for 24 h. Data are mean ± S.D., $n = 3$, $^{*}p < 0.05$ versus control cells; $\Delta p < 0.05$ versus NP group.

It was also reported the cytotoxicity of nanoparticles were associated with their particle size (Fröhlich et al., 2009; Wang et al., 2009). In this study, only the cytotoxicity of nanoparticles of 100 nm was investigated since this particle size is beneficial for mucosa binding and transport of nanoparticles (Lamprecht et al., 2001; Desai et al., 1997). Further study as to the impact of particle size on cytotoxicity of WGA–NP is needed.

Taking both cellular uptake efficiency and cytotoxicity into consideration, WGA/maleimide molar ratio at 1:10 was optimized. Our findings may provide valuable information for the rational design of nanocarriers as highly selective and effective therapeutic modalities.

4. Conclusion

WGA–NP with different WGA density were prepared and characterized in present study. Compared with NP, the modification of WGA on NP significantly promoted the cellular uptake. WGA–NP prepared at WGA/maleimide molar ratio of 1:10 exhibited the most efficient uptake and mild cytotoxicity, therefore, this molar ratio was found to be within the optimal range. These results strongly suggest that WGA density of WGA–NP play an important role in efficient cellular uptake.

Acknowledgements

The authors wish to thank Dr. Xu Qingfang for checking the English usage in preparing the manuscript. This work was supported by National Natural Science Foundation of China (no.30772657), National Basic Research Program of China (no. 2007CB935802), Special Project for Nano-technology from Shanghai (No. 0852nm04500) and National Science and Technology Major Project (2009ZX09310-006).

References

Agu, R., Dang, H.V., Jorissen, M., Willems, T., Vandoninck, S.V., Lint, J., Vandenheede, J.V., Kinget, R., Verbeke, N., 2003. In vitro polarized transport of L-phenylalanine in human nasal epithelium and partial characterization of the amino acid transporters involved. Pharm. Res. 20, 1125–1132.

Audus, K.L., Bartel, R.L., Hidalgo, I.J., Borchardt, R.T., 1990. The use of cultured epithelial and endothelial cells for drug transport and metabolism studies. Pharm. Res. 7, 435–451.

Cecarini, V., Gee, J., Fioretti, E., Amici, M., Angeletti, M., Eleuteri, A.M., Keller, J.N., 2007. Protein oxidation and cellular homeostasis: emphasis on metabolism. Biochim. Biophys. Acta 1773, 93–104.

Davda, J., Labhasetwar, V., 2002. Characterization of nanoparticle uptake by endothelial cells. Int. J. Pharm. 233, 51–59.

Desai, M.P., Labhasetwar, V., Walter, E., Levy, R.J., Amidon, G.L., 1997. The mechanism of uptake of biodegradable microparticles in Caco-2 cells is size dependent. Pharm. Res. 14, 1568–1573.

Dhuria, S.V., Hanson, L.R., Frey 2nd, W.H., 2010. Intranasal delivery to the central nervous system: mechanisms and experimental considerations. J. Pharm. Sci. 99, 1654–1673.

Dimova, S., Brewster, M.E., Noppe, M., Jorissen, M., Augustijns, P., 2005. The use of human nasal in vitro cell systems during drug discovery and development. Toxicol. In Vitro 19, 107–122.

Donovan, M.D., Flynn, G.L., Amidon, G.L., 1990. Absorption of polyethylene glycols 600 through 2000: The molecular weight dependence of gastrointestinal and nasal absorption. Pharm. Res. 7, 863–868.

Fakhari, A., Baoum, A., Siahaan, T.J., Le, K.B., Berkland, C., 2010. Controlling ligand surface density optimizes nanoparticle binding to ICAM-1. J. Pharm. Sci. [Epub ahead of print].

Foster, K.A., Avery, M.L., Yazsanian, M., 2000. Characterization of the Calu-3 cell line as a tool to screen pulmonary drug delivery. Int. J. Pharm. 208, 1–11.

Fröhlich, E., Samberger, C., Kueznik, T., Absenger, M., Roblegg, E., Zimmer, A., Pieber, T.R., 2009. Cytotoxicity of nanoparticles independent from oxidative stress. J. Toxicol. Sci. 34, 363–375.

Gao, X., Tao, W., Lu, W., Zhang, Q., Zhang, Y., Jiang, X., Fu, S., 2006. Lectin-conjugated PEG-PLA nanoparticles: preparation and brain delivery after intranasal administration. Biomaterials 27, 3482–3490.

Gao, X., Wu, B., Zhang, Q., Chen, J., Zhu, J., Zhang, W., Rong, Z., Chen, H., Jiang, X., 2007. Brain delivery of vasoactive intestinal peptide enhanced with the nanoparticles conjugated with wheat germ agglutinin following intranasal administration. J. Control. Release 121, 156–167.

Garg, A., Tisdale, A.W., Haidari, E., Kokkoli, E., 2009. Targeting colon cancer cells using PEGylated liposomes modified with a fibronectin-mimetic peptide. Int. J. Pharm. 366, 201–210.

Gu, F., Zhang, L., Teply, B.A., Mann, N., Wang, A., Radovic-Moreno, A.F., Langer, R., Farokhzad, O.C., 2008. Precise engineering of targeted nanoparticles by using self-assembled biointegrated block copolymers. Proc. Natl. Acad. Sci. USA 105, 2586–2591.

Ishikawa, H., Isayama, Y., 1987. Evidence for sialyl glycoconjugates as receptors for *Bordetella bronchiseptica* on swine nasal mucosa. Infect. Immun. 55, 1607–1609.

Kroll, A., Pillukat, M.H., Hahn, D., Schnekenburger, J., 2009. Current in vitro methods in nanoparticle risk assessment: limitations and challenges. Eur. J. Pharm. Biopharm. 72, 370–377.

Lamprecht, A., Schäfer, U., Lehr, C.M., 2001. Size-dependent bioadhesion of micro- and nanoparticulate carriers to the inflamed colonic mucosa. Pharm. Res. 18, 788–793.

Legen, I., Zakelj, S., Kristl, A., 2003. Polarised transport of monocarboxylic acid type drugs across rat jejunum in vitro: the effect of mucolysis and ATP-depletion. Int. J. Pharm. 256, 161–166.

Lehr, C.M., 2000. Lectin-mediated drug delivery: the second generation of bioadhesives. J. Control. Release 65, 19–29.

Lin, W., Huang, Y.W., Zhou, X.D., Ma, Y., 2006. In vitro toxicity of silica nanoparticles in human lung cancer cells. Toxicol. Appl. Pharmacol. 217, 252–259.

Lu, W., Zhang, Y., Tan, Y.Z., Hu, K.L., Jiang, X.G., Fu, S.K., 2005. Cationic albumin-conjugated pegylated nanoparticles as novel drug carrier for brain delivery. J. Control. Release 107, 428–448.

Lustig, S., Pluznik, D.H., 1976. Sensitivity of murine hemopoietic stem cells to lectin cytotoxicity. Exp. Hematol. 4, 19–26.

Macvinishl, J., Cope, G., Ropenga, A., 2007. Chloride transporting capability of Calu-3 epithelia following persistent knockdown of the cystic fibrosis transmembrane conductance regulator, CFTR. Br. J. Pharmacol. 150, 1055–1065.

Mallants, R., Vlaeminck, V., Jorissen, M., Augustijns, P., 2009. An improved primary human nasal cell culture for the simultaneous determination of transepithelial transport and ciliary beat frequency. J. Pharm. Pharmacol. 61, 883–890.
Mistry, A., Stolnik, S., Illum, L., 2009. Nanoparticles for direct nose-to-brain delivery of drugs. Int. J. Pharm. 379, 146–157.
Olivier, V., Meisen, I., Meckelein, B., Hirst, T., Peter-Katalinic, J., Schmidt, M., Frey, A., 2003. Influence of targeting ligand flexibility on receptor binding of particulate drug delivery systems. Bioconjug. Chem. 14, 1203–1208.
Panyam, J., Labhasetwar, V., 2003. Dynamics of endocytosis and exocytosis of poly(d,l-lactide-*co*-glycolide) nanoparticles in vascular smooth muscle cells. Pharm. Res. 20, 212–220.
Reynoso-Camacho, R., Gonzalez De Mejia, E., Loarca-Pina, G., 2003. Purification and acute toxicity of a lectin extracted from tepary bean (*Phaseolus acutifolius*). Food Chem. Toxicol. 41, 21–27.
Sarkar, M.A., 1992. Drug metabolism in the nasal mucosa. Pharm. Res. 9, 1–9.
Schipper, N.G.M., Verhoef, J.C., Merkus, F.W.H.M., 1991. The nasal mucociliary clearance: Relevance to nasal drug delivery. Pharm. Res. 8, 807–814.
Schwarz, R.E., Wojciechowicz, D.C., Picon, A.I., Schwarz, M.A., Paty, P.B., 1999. Wheat germ agglutinin-mediated toxicity in pancreatic cancer cells. Br. J. Cancer 80, 1754–1762.
Sun, H., He, X.H., Huang, B.Y., Xu, L.H., Cheng, Y.H., Zeng, Y.Y., 2001. Induction of apoptosis by wheat germ agglutinin in mouse fibroblast cell line L929. Chin. J. Pathophysiol. 17, 602–605.
US Pharmacopeia XXXII, 2009. US Pharmacopeial Convention, Rockville, MD, pp. 97.
Vila, A., Sanchez, A., Evora, C., Soriano, I., McCallion, O., Alonso, M.J., 2005. PLA–PEG particles as nasal protein carriers: the influence of particle size. Int. J. Pharm. 292, 43–52.
Wang, F., Gao, F., Lan, M., Yuan, H., Huang, Y., Liu, J., 2009. Oxidative stress contributes to silica nanoparticle-induced cytotoxicity in human embryonic kidney cells. Toxicol. In Vitro 23, 808–815.
Wang, G.H., Jiang, Z.L., Chen, Z.Q., Li, X., Peng, L.L., 2010. Neuroprotective effect of L-serine against temporary cerebral ischemia in rats. J. Neurosci. Res. 88, 2035–2045.
Weissenböck, A., Wirth, M., Gabor, F., 2004. WGA-grafted PLGA-nanospheres: preparation and association with Caco-2 single cells. J. Control. Release 99, 383–392.
Werner, U., Kissel, T., 1996. In-vitro cell culture models of the nasal epithelium: a comparative histochemical investigation of their suitability for drug transport studies. Pharm. Res. 13, 978–988.
Witschi, C., Mrsny, R.J., 1999. In vitro evaluation of microparticles and polymer gels for use as nasal platforms for protein delivery. Pharm. Res. 16, 382–390.
Yang, H., Liu, C., Yang, D., Zhang, H., Xi, Z., 2009. Comparative study of cytotoxicity, oxidative stress and genotoxicity induced by four typical nanomaterials: the role of particle size, shape and composition. J. Appl. Toxicol. 29, 69–78.
Yeeprae, W., Kawakami, S., Yamashita, F., Hashida, M., 2006. Effect of mannose density on mannose receptor-mediated cellular uptake of mannosylated O/W emulsions by macrophages. J. Control. Release 114, 193–201.